

Temperature evolution in a WC-6% Co cutting tool during turning machining : experiment and finite element simulations

Tchadja Kagnaya, Myriam Lazard, Laurence Lambert, Christine Boher, Thierry Cutard

▶ **To cite this version:**

Tchadja Kagnaya, Myriam Lazard, Laurence Lambert, Christine Boher, Thierry Cutard. Temperature evolution in a WC-6% Co cutting tool during turning machining : experiment and finite element simulations. WSEAS Transactions on Heat and Mass Transfer, 2011, 6 (3), pp.71-80. hal-01847794

HAL Id: hal-01847794
https://hal.science/hal-01847794

Submitted on 25 Sep 2018

HAL is a multi-disciplinary open access archive for the deposit and dissemination of scientific research documents, whether they are published or not. The documents may come from teaching and research institutions in France or abroad, or from public or private research centers.

L'archive ouverte pluridisciplinaire **HAL**, est destinée au dépôt et à la diffusion de documents scientifiques de niveau recherche, publiés ou non, émanant des établissements d'enseignement et de recherche français ou étrangers, des laboratoires publics ou privés.

Temperature evolution in a WC-6%Co cutting tool during turning machining: experiment and finite element simulations

T. KAGNAYA [1,2], M. LAZARD [2,3], L. LAMBERT [2], C. BOHER [1], T. CUTARD [1]

[1] Toulouse University, Institut Clément Ader, Ecole Mines Albi, F-81013 Albi cedex, FRANCE

[2] Laboratoire d'Energétique et de Mécanique Théorique et Appliquée, LEMTA CNRS-UMR 7563, Ecole Nationale Supérieure des Mines de Nancy, (ENSMN), GIP-InSIC, 27 rue d'Hellieule, 88100, Saint-Dié-des-Vosges, FRANCE

[3] Institut PPrime UPR 3346, Département Thermique, Fluide et Combustion, Ecole Nationale Supérieure d'Ingénieurs de Poitiers (ENSIP), Bâtiment B25, Campus Sud, 2 rue Pierre Brousse, 86000 Poitiers, FRANCE

tchadja.kagnaya@mines-albi.fr

Abstract: - The present paper focuses on thermal simulations and temperature measurements in a cutting tool during the machining process. The experimental studies deal with turning an AISI 1045 steel with cemented carbide insert (WC-%6Co). During machining, transient temperatures are measured at two points in cutting tool using the embedded thermocouple method. Three cutting force components are simultaneously recorded. The thermal simulations are based on the calculation of the heat flux from cutting forces and heat partition coefficient. Results obtained by thermal simulations are in good agreement with experimental ones.

Key-Words: - turning machining, WC-%6Co, tool/chip contact, temperature, heat transfer

1 Introduction

The machining cost depends on the metal removal rate which is strongly dependent on the tool life and on cutting conditions (cutting speed, feed rate, cutting environment). Generally, increasing the metal removal rate means to increase cutting parameters. However, there is plenty of evidence in literature that machining processes generate an important heat and the temperature has a great influence on cutting tool wear since it modifies the thermal, mechanical, thermomechanical and metallurgical properties [1–7]. Moreover, the temperature becomes more a critical tool wear parameter in high speed machining. Consequently, to reduce cutting tool temperature, cutting fluids are generally used. However, their use generates other constraints which are: worn fluids and chips treatment, effects on the health of operators, effects on the environment. Indeed it should be noted that the cutting fluids cost remains high [8, 9]. Moreover, Childs [10] and Li [11] show that for high speeds machining, the lubrication has a least influence on the tool-chip and tool-workpiece friction conditions. Actually, dry machining techniques are extensively studied for a better understanding of tool wear mechanisms, specially the influence of temperature. Extensive efforts have been made to obtain a cutting tool temperature, however there are real difficulties to obtain an accurate temperature since metal cutting is a coupled thermo-mechanical process. Although, lots of efforts in theoretical analyses and experiments [12, 13] have been made to understand this phenomenon, many problems are still remaining unsolved. One of these problems deals with heat transfer at tool contact interfaces. Various experimental techniques (thermocouple, infrared system, etc.) have been developed and used to evaluate the cutting temperature during machining operations; however, main of these techniques allow to obtain the temperature within the tool. They allow to follow the cutting tool temperature evolution according to the time at a point or at a given subdomain under the friction surface. Furthermore, recording temperatures allow to estimate the tool contact temperature by

approximation too. Indeed it is well known that only the knowledge of the tool contact temperature allows a better understanding of the tribological contact interface behavior. However, errors on these extrapolated temperatures are sometimes high and can involve approximation interpretations. So to complete the experimental studies, analytical, numerical and hybrid (experimental-computational) models are developed. Komanduri and Hou [14–16] made reviews of analytical methods. They proposed analytical models considering the principal heat sources: the primary shear zone and the secondary shear zone (or tool-chip friction zone). They pointed out that, taking into account those two principal heat sources, allows to predict accurately the temperature distribution in the tool. These models take into account the effect of each heat sources. Moufki and al [17] proposed an analytical model to obtain tool/chip interface temperature. They assumed that all the heat generated at the tool/chip interface flows into chip according of Boothroyd's [18] assumption. This assumption uppredicted tool/chip interface temperature. Moreover, the influence of the convection is neglected in the model. In spite of simplifying assumptions of analytical models, they have been providing the capital information for the thermal aspects of the metal cutting and have been continuously improved by eliminating simplifications and by applying refining assumptions. Today, numerical simulations for investigating cutting tool temperature are remarkably increasing because these simulations allow to obtain quite interesting results as local or global temperatures in cutting tool. The numerical simulations take into account the complex tool geometry and boundary conditions. However, thermomechanical simulations are strongly influenced by workpiece material behavior law and other parameters related to the numerical methods (damage law, formulation of finite elements). Consequently, the temperatures predicted by this method must be analyzed with attention. Davies and al [19] showed the influence of workpiece material behavior law on the cutting tool temperature obtained by finite elements methods. Their results showed that when the Johnson-Cook materials behavior law is used in thermomechanical simulations, numerical tool temperature is underestimated among 180°C and 380°C while the using power material behavior law underestimated the cutting tool temperature among 20°C to 100°C compared to experimental measurements. Moreover, the thermomechanical simulations cutting time is, in fact, about 2 or 3 orders lower than the time necessary to reach steady-state conditions due to the required CPU time as pointed out Filice [20]. In fact, pure thermal simulations allow to predict a more accurate tool temperature [19, 21]. Davies and al showed that using the pure thermal simulations based on the finite difference method, the computational temperature is in a good agreement with the experimental results compared to thermomechanical simulations.

In the present paper, a pure thermal numerical modeling approach is employed to obtain the temperature distribution in the cutting tool during machining of medium AISI 1045 steel. The hybrid method is used in this thermal numerical modeling. In fact the heat flux is calculated using the cutting forces measured during machining. The predicted temperature distribution in the tool is compared to tool temperatures measured using embedded thermocouples.

2 Experimental procedure

Fig.1 shows the experimental setup for machining. All experimentswere carried out on a CNC REALMECA T400 device.

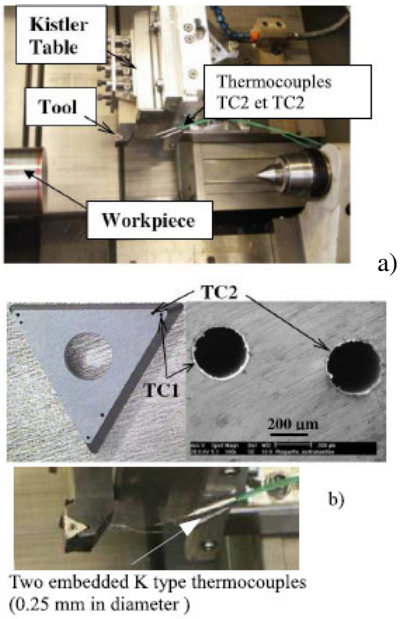


Figure 1: a) Experimental setup,
b) Detail of the WC-6%Co cutting insert (holes for TC1and TC2 locations)

The material used in experimental tests was AISI 1045 steel in the form of cylindrical bars. The thermophysical properties of AISI 1045 are detailed in Table 1.

Conductivity, k_w (W/m °C)	54

Specific heat, c_w (J/Kg °C)	480
Density, ρ_w (kg/m^3)	7800

Table 1: Thermophysical properties of the steel

Commercial uncoated cutting tool inserts TCMW 16T304 (ISO K20 and G1 grade) were used without coolant. The tool holder has the standard ISO designation STGCL 2525M16. Geometry characteristics and physical properties of tool insert and of tool holder are detailed in Table 2.

Geometry of the tool insert						
Rake angle (°C)				0		
Flank angle (°C)				6		
Thermophysical properties of tool insert						
Temperature (°C)	20	100	200	300	500	600
k_t (W/m °C)	117	110	97	86	85	83
c_t (J/Kg °C)				222		
ρ_t (kg/m^3)				14900		
Thermophysical properties of tool holder						
k_{th} (W/m °C)				42		
c_{th} (J/Kg °C)				473		
ρ_{th} (kg/m^3)				7850		

Table 2: Geometry and physical properties of tool insert and of tool holder

Three cutting speeds of 250, 300 and 400 m/min, a feed rate of 0.1 mm/rev and a depth of cut of 1.1 mm were retained for experimental tests. For each machining test, a new tool insert is used, so that the cutting forces and cutting tool temperature are measured during all machining tests. The cutting forces are measured using a Kistler 9257B piezoelectric dynamometer. The dynamometer, equiped with three load cells, is used to measure the main cutting force Fc, feed force Ff and radial force Fp. In order to measure temperature, two thermocouples (K types) of diameter 0.25 mm are embedded in the cutting insert (Fig.1(b)). The first thermocouple (TC1) is located near from the tool/chip interface (rake face) and a second one (TC2) near from the tool/workpiece interface (flank face). Holes in the cutting insert were obtained by electro-discharge machining (EDM). The predicted temperature distribution in the tool is compared to tool temperatures measured using embedded thermocouples.

3 Finite Element Simulation

3.1 Heat Flux calculation

The thermal numerical model proposed in this works allows to calculate a temperature in the cutting tool. The model is based on consideration of the thermal heat flux. The heat flux is calculated using cutting force measurements during machining tests. The heat flux generated in the cutting process is mainly due to three cutting zones: the primary shear zone, the tool/workpiece interface and the secondary shear zone (tool/chip interface). However, various studies showed that most of the heat (90%) generated in the primary zone is removed into the chip while the remaining part is undergoing in the workpiece [22, 23]. This consideration is more justified at high speeds and for dry machining since the adiabatic phenomenon appears in the primary shear zone under such conditions. According to this phenomenon, the cutting tool temperature is mainly due to friction zones (tool/chip and tool/workpiece interfaces). In the friction contact problem, heat transfer is moreover complex since the contact surfaces are not perfect. Consequently, the heat transfer at contact interfaces depends on many parameters and conditions such as contact type, surface properties, and pressures. Irregular or small contact areas between two surfaces create thermal contact resistances and the constriction phenomenon occurs. As a consequence, it appears a high local temperature at small contact areas. For numerical thermal simulations, it is difficult to take into account the constriction resistance phenomenon.

In the present work, the following assumptions are considered:

- Influence of the heat generated in the primary shear zone is neglected (adiabatic phenomenon),
- Tool/workpiece contact area is very small because of the constriction resistance phenomenon at this interface. Thus, the thermal heat transfer through this area is neglected since it can introduce an important error in calculation results,
- Only the heat flux generated by friction at the tool/chip interface is considered,
- Only one type of tool/chip contact exists (sliding contact). The sticking contact which can exist near the cutting edge is neglected,
- The tool/chip contact pressure and consequently the heat flux is uniformly distributed (perfect contact).

Machining tests are carried out in the three-dimensional-orthogonal configuration. Obviously the cutting speed is orthogonal to the cutting edge.

However the influence of tool nose radius on the cutting forces is neglected since al large depth of cut is considered compared to the feed speed and to the tool nose radius (lower than 0.4 mm).

The power dissipated at the tool/chip interface ($Q_{fr}(t)$) is calculated according to the interface tool/chip friction force ($F_{fr}(t)$) and chip flow velocity (V_{ch}) Eq.(1). It is important to note that the dissipated power is calculated for each recording time according to measured cutting forces.

$$Q_{fr}(t) = F_{fr}(t)V_{ch} \quad (1)$$

The tool/chip friction force ($F_{fr}(t)$) and the chip flow velocity (V_{ch}) are calculated using respectively Eqs.(2) and (3):

$$F_{fr}(t) = \left(F_f^{\,2}(t) + F_p^{\,2}(t)\right)^{1/2} \quad (2)$$

$$V_{ch} = V_c \frac{\sin\phi}{\cos(\phi - \alpha)} \quad (3)$$

where F_f is the orthogonal cutting force, F_p is the radial cutting force, V_c the cutting speed, α is the rake angle, and ϕ the shear angle.

It is well known that chip flow velocity depends on the shear angle ϕ and on the friction angle γ which are calculated with Eqs.(4) and (5):

$$\phi = \frac{\pi}{4} - \frac{\gamma - \alpha}{2} \quad (4)$$

$$\gamma = \tan^{-1}\left(\frac{F_{fr}}{F_c}\right) \quad (5)$$

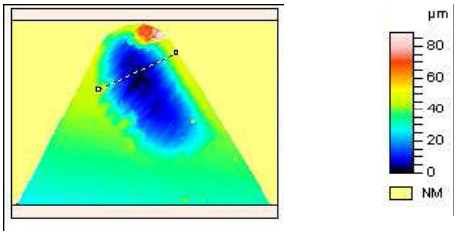
where F_c is the tangential cutting force.

Using, the power dissipated at tool/chip interface Eq.(1), the heat flux in the friction zone ϕ_{fr} can be calculated with Eq.(6):

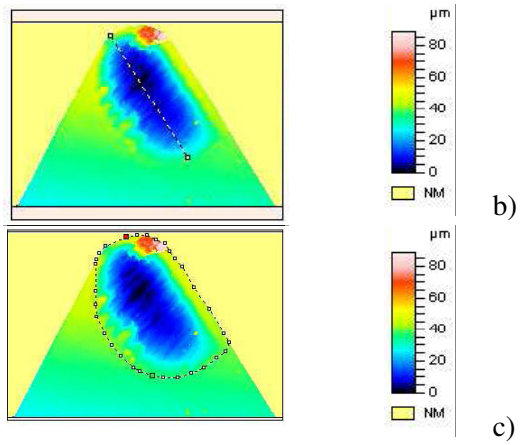
$$\varphi_{fr}(t) = \frac{Q_{fr}(t)}{Sc} \quad (6)$$

where *Sc* is the tool/chip contact area.

As it can be observed from Eq.(1), the heat flux highly depends on the tool/chip contact area. Thus, the chip/tool contact area determination represents one of the most capital and delicate step. In this work, the average tool/chip contact area is determined using a confocal microscope (Fig.2).



a)



b)

c)

Figure 2: Example of contact surface characteristics measurement:
a) contact length,
b) contact width
c) contact surface (case of Vc = 400 m/min, f = 0.1mm/rev et doc =1.1 mm)

The heat flux generated at the tool/chip interface is transmitted on the one hand in the cutting tool and on the other hand in the chip. The heat partition coefficient for the cutting tool is calculated by following relationship
(Eq.(7)):

$$\beta_{tool} = 1 - \beta_w \quad (7)$$

The heat partition coefficient for the chip (w) is evaluated using the relationship of Shaw [24] Eq.(8):

$$\beta_{tool} = 1 - \left\{1 + \left[0,754\left(k_t / k_w\right)\left(A_a\sqrt{N_T}\right)^{-1}\right]\right\}^{-1} \quad (8)$$

As previously mentionned, the tool/chip contact area plays an essential role in the calculation of the heat flux, thus it is important to take into account the tool/chip contact geometry factor. The relation suggested by Loewen [26] Eq.(10) to calculate Aa is complex and in the present work, a simplified relationship is proposed. Here, A_a only depends on the ratio between the depth of cut (w) and the tool/chip contact length (lc) as follow Eq.(11):

$$N_T = \frac{V_{ch} lc}{a_w} \quad (9)$$

$$A_a = \frac{2}{\pi}\left[\sinh^{-1}\left(\frac{m}{l}\right) + \frac{m}{l}\sinh^{-1}\left(\frac{l}{m}\right) + \frac{1}{3}\left(\frac{m}{l}\right)^2 \ldots + \frac{1}{3}\frac{l}{m} - \frac{1}{3}\left(\frac{m}{l} + \frac{l}{m}\right)\left(1 + \left(\frac{m}{l}\right)^2\right)^{1/2}\right] \quad (10)$$

Finally heat flux dissipated into the cutting tool can be calculated by Eq.(13) by combining Eqs.(7), (11) and Eq.(12). It allows to calculate the heat

proportion coefficient (tool) for the tool using Eqs.(8) and (11):

$$A_a = \frac{w}{lc} \qquad (11)$$

Eq.(13) shows that the heat flux depends on the thermal conductivities of the cutting tool and the workpiece. The thermal conductivity of the cutting tool depends on the temperature (Table 2). To study the influence of the cutting tool thermal conductivity on the heat flux, three values have been considered: 117, 100 and 83 W/m°C. These three values are respectively named k_{sup}, k_{med}, and k_{inf} . k_{sup} corresponds to the highest value measured at ambient temperature (20°C), k_{med} is a median value which is close to the mean conductivity (k_{moy} = 96.33 W/m°C) of all measured values and k_{inf} corresponds to the lower conductivity value obtained at high temperature (600°C).

Fig.3 shows the evolution of the tool/chip contact geometry factor. The curve 1 is obtained by using Loewen's relationship Eq.(10) and curve 2 by considering Eq.(11). A good agreement can be observed between these two curves.

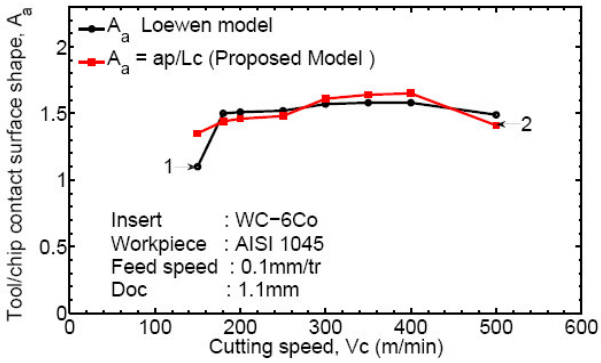


Figure 3: Evolution of tool/chip contact surface shape vs cutting speed

Fig.4 illustrates the evolution of the heat partition coefficient (tool) versus the cutting speed.

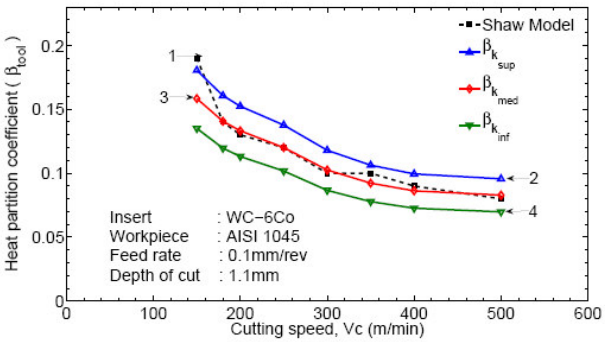


Figure 4: Evolution of heat partition coefficient vs cutting speed for different conductivity values

Curve 1 is obtained by using the model of Shaw [24]. It must be noticed that only the (k_{med}) conductivity value is considered in that case. Curves 2 to 4 are obtained while considering the modified model proposed in the present paper according to the three thermal conductivity values (k_{sup}, k_{med}, and k_{inf}). It can be observed that when the cutting speed increases, tool decreases. This evolution is mainly due to the decrease of ($A_a N_T^{1/2} = (w/lc) N_T^{1/2}$) when the cutting speed increases. Eq.(3) shows that the chip flow speed increases when the cutting speed increases. This means that the decrease of $(V ch/lc)^{1/2}$ is more due to a high rate decrease of the tool/chip contact length when the cutting speed increases [27]. Fig.4 shows a significant influence of the thermal conductivity on the heat partition coefficient: it increases when the thermal conductivity is high (i.e. at low temperature). A good correlation is observed between the evolutions of the heat partition coefficient obtained for both models when using k_{med}. The three values of the heat partition coefficient are used for the thermal simulation.

3.2 Boundary conditions

The cutting tool geometrical model built for the tool holder, the insert support (shim) and the insert is represented in Fig.5(a). This model is used in the finite elements code Abaqus 6.7/Standard to compute the cutting tool temperature fields. Fig.5(b) shows the detail of boundary conditions for on the cutting tool insert. The heat flux is imposed at the tool/chip contact area ($w \times lc$). As mentioned before, the imposed heat flux depends on time.

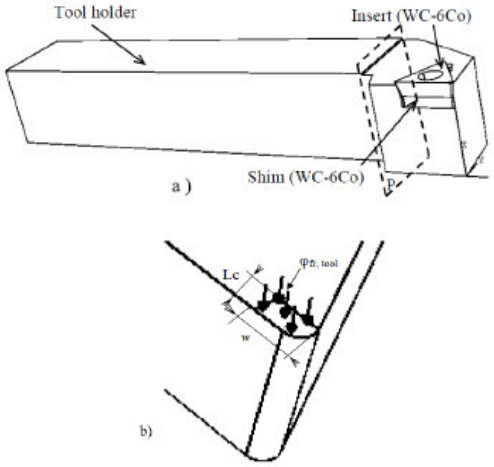


Figure 5: a) Insert, shim and tool holder;
b) Detail for heat boundary conditions

As an example, the average heat flux dissipated in the cutting tool for the following cutting speeds of

250, 300 and 400 m/min is respectively of 67, 81 and 79 MW/m^2 when considering β_{tool} in case of k_{med}.

The cutting tool geometrical model is divided in two parts by the plan (P) (Fig.5(a)).

Boundary conditions are defined by considering the following assumptions:

• It is supposed that the part located on the left of plan (P) is far away

from the heat source and remains at room temperature (20°C). The free faces located on the right of plan (P) (in contact with the air) are subjected to a forced convection due to the workpiece rotation. The heat exchange coefficient (h_f) is obtained by using Nusselt´s empirical correlation formulas,

• It is supposed that the tool-holder/shim and shim/insert contacts are

perfect (perfect heat conduction),

• The tool/chip contact surface is considered as being constant. Consequently, the evolution of wear is not taken into account properly in the model. But the tool wear is indirectly taken into account since measured cutting forces include the effects of wear phenomena.

The heat transfer coefficient by forced convection (hf) is given by Eq.(14) [28]:

$$h_f = \frac{k_{air} Nu}{d_{t-h}} \quad (14)$$

where k_{air} is the thermal conductivity of air (0.0262W/m°C), d is the characteristic length of tool the holder (25 mm) and Nu is the Nusselt correlation number (Eq.(15)) which depends on the Reynolds number Re (Eq.(16)).

$$Nu = C\,\mathrm{Re}^m \quad (15)$$

$$\mathrm{Re} = \frac{\rho_{air} d_{t-h} V_c}{\nu_{air}} \quad (16)$$

where C and m are constants (C = 0.27 and m = 0.66), β_{air} is the air density (1.290 kg/m^3), V_c is the cutting speed and ν_{air} is the dynamic viscosity (1.8 $^{-5}$ kg m^{-1} s^{-1}). The heat transfer problem is solved in a transient case by taking into account all the boundary conditions and the thermal properties given in Table 1 and Table 2. The heat transfer coefficient by forced convection (h_f) and the temperature dependence of the cutting insert thermal conductivity is incorporated in thermal simulations. The geometrical model of the whole cutting tool is meshed by using tetrahedral triangular elements DC3D4. The shim and cutting insert are meshed respectively by 50713 and 214000 elements, while the tool holder is meshed by 75383 elements.

4 Results and discussion

4.1 Experimental results

Fig.6 shows an example of the evolution of cutting tool temperatures recorded by thermocouples for the cutting speed of 300 m/min.

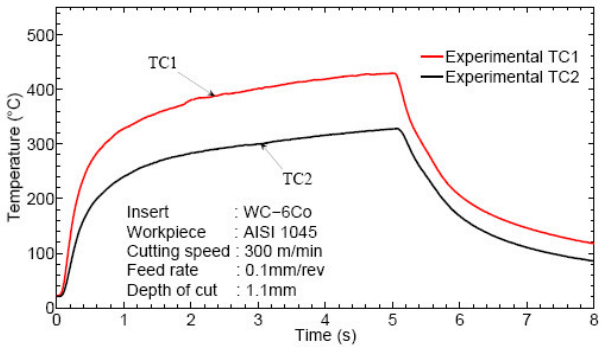


Figure 6: Evolutions of the cutting tool temperature vs time (V_c = 300 m/min)

For machining times greater than one second (Fig.6), the temperature increases slightly. This phenomenon can be explained by considering two phenomena. On the one hand, the heat flux generated during machining tests becomes constant; on the other hand tool wear reduces the distance between thermocouples and the heat source. The maximum temperature levels recorded by thermocouples TC1 and TC2 are respectively close to 420°C and to 320°C. Similar temperature levels are obtained by Filice et al. [20] by machining a medium AISI 1045 steel with a WC-%6Co insert and for a cutting speed of 200 m/min, a feed rate of 0,2 mm/rev. and a depth of cut of 3 mm.

Fig.7 represents the maximum temperatures versus the cutting speed. It can be observed that the cutting temperature increases as the cutting speed increases.

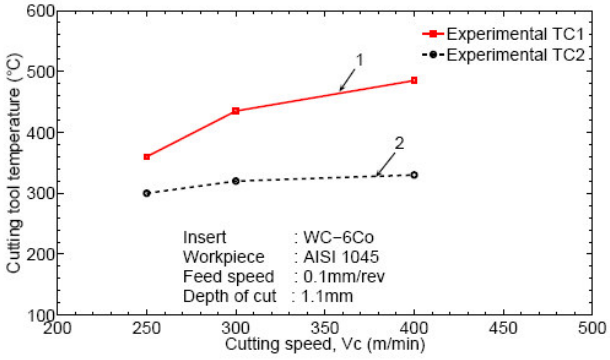


Figure 7: Evolutions of cutting tool temperature vs cutting speed

It is clearly shown in the literature that the cutting forces increase when the cutting speed increases, thus the generated heat (i.e temperature) increases. The temperature recorded by the thermocouple TC1, which is closer to the tool/chip contact, increases significantly with the cutting speed while the one recorded by thermocouple TC2 increases slightly. The maximum temperature recorded by thermocouples TC1 and TC2 are respectively of 480°C and 340°C. Such temperature levels in the cutting tool can lead to soften the tool material.

4.2 Comparison between experimental and numerical results

The thermal simulations presented above allow to estimate the cutting tool temperature field and the tool/chip interface temperature. Fig.8 shows an example of the temperature distribution in a cutting tool in the case of a cutting speed equal to 250 m/min, while considering the thermal conductivity k_{med}. Fig.8 shows that isotherms have a geometry close to a spherical form as previously observed by Liu and Chou [29] and Filice et al. [20].

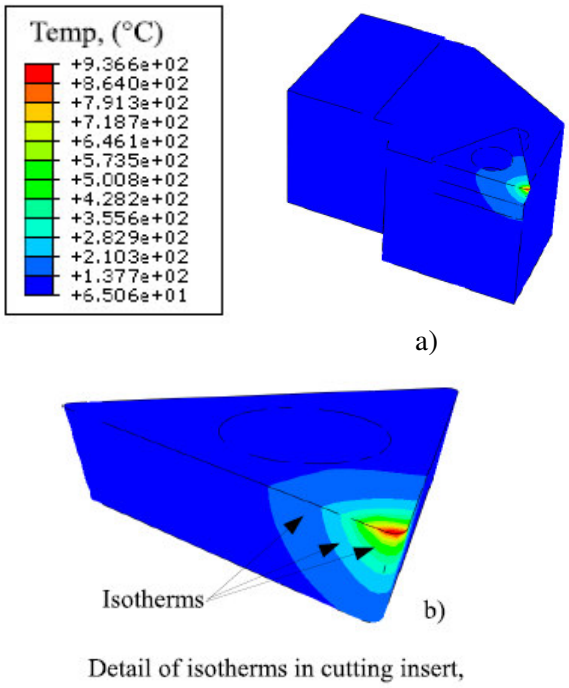


Figure 8: Temperature distribution in the cutting tool (Vc = 250m/min, f=0,1mm/tr, ap=1,1mm).

Numerical cutting tool temperatures are compared with the temperature measurements too. Numerical temperature values are extracted at the thermocouple location points. Fig.9 shows the comparison between simulated and measured tool temperatures for the cutting speed of 300 m/min and for the TC1 thermocouple.

Numerical tool temperature values are in good agreement with experimental ones when considering the k_{med} thermal conductivity value. For this case, the error is less than 3% for thermocouple TC1, when the cutting tool temperature is in a quasi steady-state domain. Fig.9 shows the influence of the cutting tool thermal conductivity on numerical temperatures.

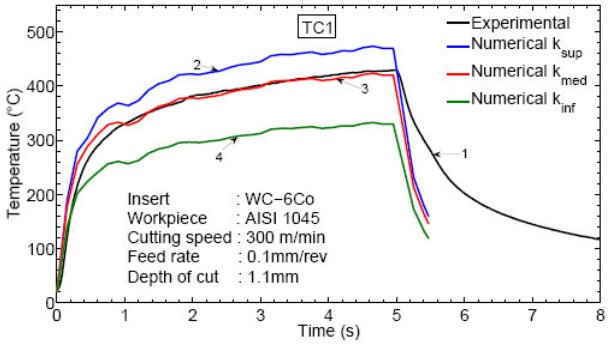


Figure 9: Comparison of experimental (1) and numerical temperatures (2, 3, 4) for different conductivity values (Thermocouple TC1).

The higher the conductivity is, the more the calculated tool temperature is. This phenomenon must be related to the fact that the heat flux is related to the tool conductivity through the heat partition coefficient. The maximum mismatches between temperatures calculated on the one hand by considering conductivities k_{med} and k_{sup} and on the other hand by considering conductivities k_{inf} and k_{med} are respectively of 35°C and of 66°C.

The variation obtained by considering conductivities k_{inf} and k_{med} is more important than the variation calculated by considering conductivities k_{med} and k_{sup} for the two thermocouples. This is not due to the variation of the heat partition coefficient for the same cutting speed, but is due to the fact that the thermal conductivity decreases when the temperature increases. Such a behavior was well established by Abdel-Aal et al. [30] by studying the influence of the thermal conductivity on the carbide tool wear when machining titanium based alloys. The same observation was made in the case of the tool temperature calculated or measured with TC2 (Fig.10).

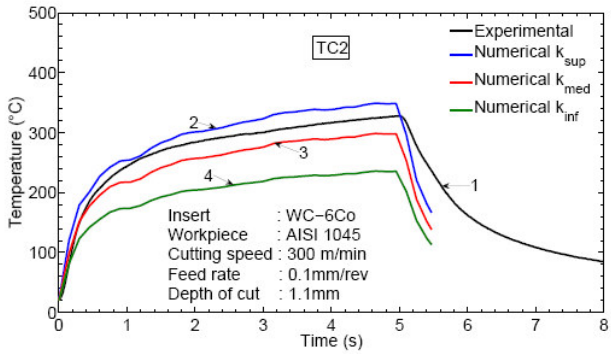


Figure 10: Comparison of experimental (1) and numerical temperatures (2, 3, 4) for different cutting insert conductivity values (Thermocouple TC2)

Fig.11(a) represents a tool/chip interface temperature cartography in the case of a cutting speed of 400 m/min by considering the thermal conductivity k_{med}. The temperature cartography allows to observe that the maximum temperature (1280°C) on the rake face is located near to the cutting edge and nearest to the cutting nose. Two temperature profiles are plotted according to the two segments drawn on the cartography (Fig.11(b)). Each profile illustrates that the temperature decreases from the cutting edge to the end of the tool/chip contact.

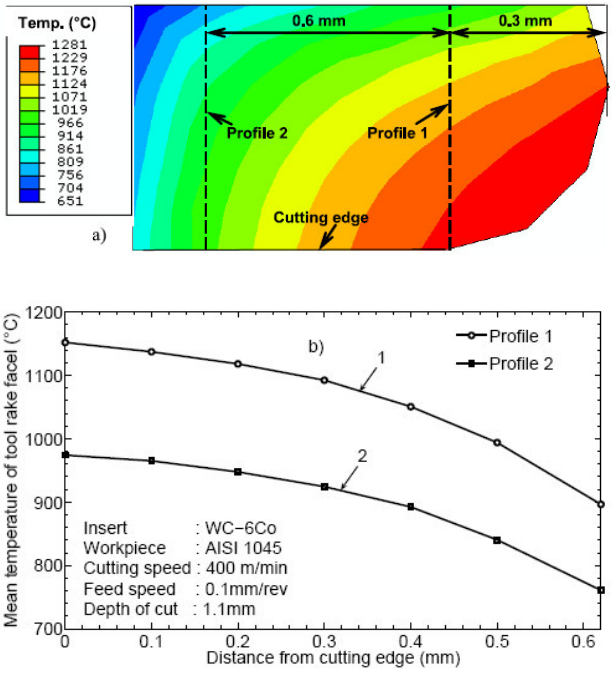


Figure 11: Calculated cutting tool temperature :
a) rake face temperature cartography ;
b) temperature profiles on the rake face (Vc = 400 m/min, f = 0.1 mm/rev, ap = 1.1 mm, time = 5 s)

Temperature varies between 900°C and 1150°C along profile 1 and the 760°C and 980°C along profile 2. Using the tool/chip interface temperature distribution for the three cutting speeds, the mean temperature of the rake face is determined.

Fig.12 plots the mean temperature of the tool rake face as a function of the cutting speed, according to the three thermal conductivity cases (k_{sup}, k_{med}, and k_{inf}). This representation allows a better identification of the level of the tool/chip interface temperature and of the conductivity influence.

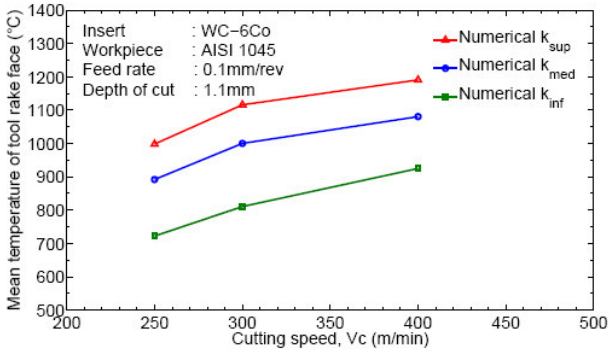


Figure 12: Evolution of the mean temperature of the tool rake face vs cutting speed for different values of cutting tool conductivity

From Fig.12, one can remark again that the higher the conductivity is, the higher the calculated tool temperature is. As observed in the experimental case, the average temperature of the tool/chip interface increases when the cutting speed increases. Considering the thermal conductivity k_{med}, the average temperatures of the tool rake face are respectively of 891°C, 1002°C and 1082°C for cutting speeds of 250 m/min, 300 m/min and 400 m/min.

The average temperature level for the rake face, obtained in the case of 250 m/min and by considering the thermal conductivity k_{med}, is in good agreement with Filice et al [20] and Grzesik and Luttervelt [31] results. Indeed, Filice et al. [20], by mean of 3D numerical simulations, obtain 900°C at the tool/chip interface with the following cutting conditions: cutting speed of 200 m/min, feed rate of 0.2 mm/rev and depth of cut of 3 mm. The average tool temperature of the rake face for 400 m/min is particularly high. Such extreme tool temperatures cause the collapse of the cutting edge and a more severe degradation of the cutting tool, following a thermo-viscoplastic behavior of the WC-%6Co [32].

5 Conclusion

Cutting tool temperatures during machining a medium AISI 1045 steel with a cemented carbide based cutting tool were studied experimentally and numerically.

Experimental results showed that the cutting tool temperature increases when the cutting speed increases. This is in good agreement with previous results presented in the literature. The maximum temperature recorded by thermocouples TC1 and TC2 at a high cutting speed (400 m/min) are respectively close to 480°C and to 340°C. Thermal simulations were carried on to estimate the cutting tool temperature distribution and the rake face temperature. The numerical model is based on the tool/chip interface heat source obtained from the cutting forces monitored during the turning process. The heat flux dissipated in the cutting tool is calculated by taking into account heat partition coefficients. The more realistic boundary conditions and the dependence to the thermal conductivity of the cutting insert are considered in thermal simulations.

Experimental temperatures are compared to these obtained numerically. Three different values are considered for the cutting tool thermal conductivity : 117 W/(m °C), 100 W/(m °C) and 83 W/(m °C). A good agreement between experimental and numerical results is obtained for a conductivity value of 100 W/(m °C). For this case, the average temperature of the tool rake face is of 891°C, 1002°C and 1082°C respectively for cutting speeds of 250 m/min, 300 m/min and 400 m/min. This study showed that the temperature of the cutting tool increases considerably when the thermal conductivity increases.

This explains that the thermal conductivity has an important effect on the tool temperature increase. It should be noticed that, the heat partition coefficient is calculated by using a constant thermal conductivity. Ideally it would be better to consider that the heat partition coefficient depends on the temperature by the means of the thermal conductivity. Thermal simulations show that the temperature levels reached during machining are high enough to modify highly the mechanical behaviour of the WC-6%Co grade. Considering such results will be helpful to obtain a better understanding of tool wear mechanisms. This is an objective of future works.

References:

[1] T. Kitagawa, A. Kubo, K. Maekawa, Temperature and wear of cutting tools in high-speed machining of Inconel 718 and Ti-6Al-6V-2Sn, Wear 202 (2) (1997) 142–148.

[2] S. K. Choudhury, G. Bartarya, Role of temperature and surface finish in predicting tool wear using neural network and design of experiments, International Journal of Machine Tools and Manufacture 43 (7) (2003) 747–753.

[3] G. List, Wear behaviour of cemented carbide tools by the characterization of the tool-chip interface: Application to dry machining of aeronautical aluminium alloy AA2024 T351, Ph.D. thesis, Ecole Nationale Supérieure des Arts et Métiers (2004).

[4] T. Kagnaya, C. Boher, L. Lambert, M. Lazard, T. Cutard, Wear mechanisms of WC-Co cutting tools from high-speed tribological tests, Wear 267 (5-8) (2009) 890–897.

[5] J. A. Arsecularatne, L. C. Zhang, C. Montross, Wear and tool life of tungsten carbide, PCBN and PCD cutting tools, International Journal of Machine Tools and Manufacture 46 (5) (2006) 482–491.

[6] M. Lazard, P. Corvisier, Modelling of a tool during turning : Analytical prediction of the temperature and of the heat flux at the tool's tip, Applied Thermal Engineering 24 (5-6), 839-849.

[7] M. Lazard, Heat Transfer during cutting process: modeling and prediction towards real time control, Chapt. 8, In: Thermal Engineering Research Developments ISBN: 978-1-60741-497-1. Editors: J. Evgova, O. Kostadinov - © 2009 Nova Science Publishers, Inc.

[8] P. Marksberry, I. Jawahir, A comprehensive tool-wear/tool-life performance model in the evaluation of ndm (near dry machining) for sustainable manufacturing, International Journal of Machine Tools and Manufacture 48 (7-8) (2008) 878–886.

[9] F. Klocke, G. Eisenblätter, Dry cutting, CIRP Annals – Manufacturing Technology 46 (2) (1997) 519–526.

[10] T. H. C. Childs, Friction modelling in metal cutting, Wear 260 (3) (2006) 310–318.

[11] K.-M. Li, Predictive modeling of near dry machining: mechanical performance and environmental, Ph.D. thesis, Georgia Institute of Technology (August 2006).

[12] N. A. Abukhshim, P. T. Mativenga, M. A. Sheikh, Heat generation and temperature prediction in metal cutting: A review and implications for high speed machining, International Journal of Machine Tools and Manufacture 46 (7-8) (2006) 782–800. 28

[13] R. Komanduri, Z. B. Hou, A review of the experimental techniques for the measurement of heat and temperatures generated in some manufacturing processes and tribology, Tribology International 34 (10) (2001) 653–682.
[14] R. Komanduri, Z. B. Hou, Thermal modeling of the metal cutting process: Part I – Temperature rise distribution due to shear plane heat source, International Journal of Mechanical Sciences 42 (9) (2000) 1715–1752.
[15] R. Komanduri, Z. B. Hou, Thermal modeling of the metal cutting process Part II: temperature rise distribution due to frictional heat source at the tool-chip interface, International Journal of Mechanical Sciences 43 (1) (2001) 57–88.
[16] R. Komanduri, Z. B. Hou, Thermal modeling of the metal cutting process Part III: temperature rise distribution due to the combined effects of shear plane heat source and the tool-chip interface frictional heat source, International Journal of Mechanical Sciences 43 (1) (2001) 89–107.
[17] A. Moufki, A. Molinari, D. Dudzinski, Modelling of orthogonal cutting with a temperature dependent friction law, Journal of the Mechanics and Physics of Solids 46 (10) (1998) 2103–2138.
[18] G. Boothroyd, Temperature in orthogonal metal cutting, Proc. Instn. Mech. Engrs 29 (1963) 789–802. 29
[19] M. Davies, Q. Cao, A. Cooks, R. Ivester, On the measurement and prediction of temperature fields in machining aisi 1045 steel, CIRP Annals Manufacturing Technology 52 (1) (2003) 77–80.
[20] L. Filice, D. Umbrello, S. Beccari, F. Micari, On the FE codes capability for tool temperature calculation in machining processes, Journal of Materials Processing Technology 174 (1-3) (2006) 286–292.
[21] A. Tay, A review of methods of calculating machining temperature, Journal of Materials Processing Technology 36 (1993) 225–257.
[22] T. Childs, K. Maekawa, T. Obikawa, Y. Yamane, Metal Machining : Theory and Applications, John Wiley & Sons Inc., 2000.
[23] E. M. Trent, P. K. Wright, Metal Cutting (Fourth Edition), Butterworth-Heinemann, 2000.
[24] M. C. Shaw, Metal cutting principles, in: Oxford, Clarendon Press, 1989.
[25] W. Grzesik, P. Nieslony, Thermophysical-property-based selection of tool protective coatings for dry machining of steels, J. Manuf. Sci. Eng. 125 (4) (2003) 689–695.
[26] E. G. Loewen, M. C. Shaw, On the analysis of cutting tool temperatures, Transactions of ASME 71 (1954) 217–231.
[27] T. Kagnaya, Identification of wear mechanisms of a WC-6%Co grade in machining by combining thermal and tribological approaches, Ph.D. thesis, High School of Mines ParisTech (September 2009) 30
[28] R. G. Ahmed, M. M. Yovanovich, Experimental study of forced convection from isothermal circular and square cylinders and toroids, J. Heat Transfer, Trans. ASME 119 (1997) 70–79.
[29] J. Liu, Y. K. Chou, Cutting tool temperature analysis in heat-pipe assisted composite machining, Journal of Manufacturing Science and Engineering: Transactions of the ASME 129 (2007) 902–910.
[30] H. Abdel-Aal, M. Nouari, M. El Mansori, Tribo-energetic correlation of tool thermal properties to wear of WC-Co inserts in high speed dry machining of aeronautical grade titanium alloys, Wear 266 (3-4) (2009) 432–443.
[31] W. Grzesik, C. van Luttervelt, Analytical models based on composite layer for computation of tool-chip interface temperatures in machining steels with multilayer coated cutting tools, CIRP Annals – Manufacturing Technology 54 (1) (2005) 91–94.
[32] G. Ostberg, K. Buss, M. Christensen, S. Norgren, H. O. Andr´en, D. Mari, G. Wahnstrom, I. Reineck, Mechanisms of plastic deformation 31 of WC-Co and Ti(C, N)-WC-Co, International Journal of Refractory Metals and Hard Materials 24 (1-2) (2006) 135–144.